



Supplement of

A combined gas- and particle-phase analysis of highly oxygenated organic molecules (HOMs) from α -pinene ozonolysis

Jian Zhao et al.

Correspondence to: Jian Zhao (jian.zhao@helsinki.fi) and Mikael Ehn (mikael.ehn@helsinki.fi)

The copyright of individual parts of the supplement might differ from the article licence.

Section S1. Comparison between AMS and SMPS Measurement

The raw measurements of aerosol mass concentration from AMS and SMPS were given in Figure S1 (a1-a3). AMS measured SOA track very well with SMPS integrated mass (assuming SOA density as 1.5 g cm^{-3}) before adding seed particles, which could be well predicted by the condensation of HOM vapors formed in the gas phase, although a factor of 1-1.3 was used to scale the modeled SOA. According to the gas-particle partitioning theory, more volatile compounds start to condense and contribute to SOA as the accumulating of SOA mass. This explains the factors applied when we compared the modeled and measured SOA for experiments No. 2&3 (about 25% and 30% more SOA formed than the sole condensation of HOM, respectively).

However, large discrepancies showed up after adding NaCl seed particles. There might be influence from heterogeneous reactions, but the main reasons for this smaller increase of measured SOA than expected (in spite of the large decrease of HOM after adding seed particles in Fig. 2) include: 1) changing of the collection efficiency (CE) of AMS as previously reported (R. Bahreini, 2005). It was pure organic aerosol but gradually changed to external and/or internal mixed particles with NaCl after seed injection. The overall phase state of particles (e.g. from liquid to solid) would change the collision behavior between particles and the vaporizer of AMS, resulting in large changes of CE (negative direction, in this case, owing to more particle bounce). 2) Higher evaporation temperature of NaCl particles than $600 \text{ }^\circ\text{C}$ (used by AMS) might have negative effects on the evaporation of SOA particles.

In order to separate SOA mass from NaCl seed particles, we combined predicted SOA mass from the kinetic model described in Section S2 with SMPS and AMS measurements, following steps: 1) using the box model to estimate expected SOA mass enhancement after adding NaCl seed particles, based on the gas phase HOM concentration and condensation sink, which predicts the SOA growth well before adding seed particles (dashed blue lines in Fig. S1). 2) Seed particle number concentrations (NaCl density of 2.17 g cm^{-3}) measured before they were added into the chamber along with the dynamic dilution inside the chamber were used to estimate its mass concentration. 3) SOA mass estimated from step 1 and NaCl mass estimated from step 2 were put together, compared to the total integrated aerosol mass from SMPS measurements. Note that a mass-weighted density of $1.65\text{-}1.77 \text{ g cm}^{-3}$ for bulk SOA mixed NaCl particles were used to convert SMPS measured number concentration to mass concentration, assuming spherical particles without internal voids. After adding seed particles, a slightly higher scale factor of 1.3-1.6 were applied for modeled SOA to be consistent with SMPS measurements, owing to enhanced condensation of more volatile compounds onto those added particle surfaces. Although the relatively good comparisons between the reconstructed particle mass and the measurements (Fig. S1 b1-b3) suggest the feasibility of this method, there are large uncertainties during the estimation (e.g. particle density and HOM concentration). Thus, we intended to show that qualitatively SMPS and AMS measurements were comparable, and the scaling factors were mainly introduced to make modeled and measured mass concentrations consistent with each other.

Section S2. Description of Box Model

S2.1 Chemical Reactions

A box model was used to simulate the steady-state concentrations of reactants and some products inside the chamber. The main chemical reactions, rate constant (at 298K, adopted from Master Chemical Mechanism, MCM (Saunders et al., 2003)), and physical parameters used in this work were summarized in Table S1. We greatly simplified the complex α -pinene and $\text{O}_3/\text{OH}/\text{NO}_3$ reactions and focused on HOM related RO_2 unimolecular and bimolecular reactions. For example, the rate constants of RO_2 intramolecular H-shift could vary several orders of magnitude depending on the number of atoms within the cyclic H-shift transition state and the chemical environment of that H atom (Bianchi et al., 2019). Thus, the autoxidation (at the microsecond level) is treated to be finished instantly in this work (Iyer et al., 2021). Then, an initial distribution of RO_2 was achieved and expressed explicitly as the first step for different oxidants (Table S1), which are comparable with previous/this chamber measurements and model parameters (Rissanen et al., 2015; Mentel et al., 2015; Kirkby et al., 2016; Kurtén et al., 2017; Molteni et al., 2019; Schervish and Donahue, 2020). However, under conditions of high concentrations of $\text{RO}_2/\text{NO}/\text{HO}_2$, the bimolecular reactions could change the distribution of peroxy radicals, because some of the RO_2 will react with another partner before they undergo further autoxidation. Therefore, the

50 model may overestimate the HOM yield under these conditions, but the monomer and dimer formation are intertwined among many chemical reactions and we did not test the sensitivity of this assumption quantitatively. Another set of reactions that is not included in the model are the semi-/intermediate-volatility organic compounds (S/IVOC) oxidation, which probably will not react with O₃ but are reactive towards OH or NO₃, thus may affect the results (Peräkylä et al., 2020). However, the near linear relationship between total gas phase HOM vs. steady state α -pinene and O₃ reaction rate indicates that ozonolysis of α -pinene dominate the HOM formation even without OH scavengers (Ehn et al., 2014; Jokinen et al., 2015). Overall, we tried to use a simplified box model as support to interpret the main process inside the chamber. More detailed and accurate kinetic parameters, including the H-shift rate constants and branching ratios of RO₂ need further work.

60 Details about the estimation of HOM monomer and dimer concentrations are described as below. RO₂ represents all kinds of peroxy radicals that are not directly related to HOM formation (they could react with another HOM related RO₂ to indirectly influence HOM formation). The subscript numbers of HOM related RO_{4,6,8,10} are numbers of O atoms in corresponding peroxy radicals (i.e. two from the initial carbonyl functional group and every extra two O atoms represents one step of further autoxidation). RO_{6,8,10} could either end up as HOM monomers forming a carbonyl from the last H-abstraction in a unimolecular way, or react with another RO_{6,8,10} to form HOM monomers, HOM dimers, or alkoxy radicals (RO, assuming that RO generated from RO_{6,8,10} will end up as HOM). However, the only way RO₄ could contribute to HOM formation is bimolecular reactions with RO_{6,8,10}, but the RO formed from this pathway are partly from RO₄ and will be taken away from the products by a subjectively determined branching factor that best fits the measurements. Note that the bimolecular reaction constants used in this work ($>1e-11$ cm³ molecule⁻¹ s⁻¹) are comparable to those used by (Molteni et al., 2019; Berndt et al., 2018), which are higher than those suggested ($< 1e-11$ cm³ molecule⁻¹ s⁻¹) in MCM (Zhao et al., 2018). The cross-reaction rate constant (RO₂^a with RO₂^b, k_{ab}) was estimated based on self-reaction rate constants of each type of RO₂ (k_a and k_b), using the formula $k_{ab} \sim 2(k_a k_b)^{0.5}$. Finally, even the unimolecular and bimolecular rate constants used to simulate the COALA chamber measurements had large uncertainties, literally, it is their relative values (competition between the wall loss and particle loss) that determined the final dimer to monomer ratios.

75 Based on the α -pinene and O₃ experiments, CO or NO_x was added to the model to investigate their effect on the distribution of HOM products. The importance of bimolecular reactions of RO₂ with HO₂ was considered for CO experiments (HO₂ terminated monomer, HOM_MonomersHO₂). For NO_x experiments, both the UV lights off and on were simulated. The photolysis rate constant of NO₂ to form NO was determined during three tests, during which only NO₂ was injected into the chamber, then NO and O₃ were formed with a molar ratio of near 1:1. Note that the UV lights (400 nm) used in this work was not enough to photolyze ozone and had very limited quantum yields for aldehydes.

S2.2 Other Parameters

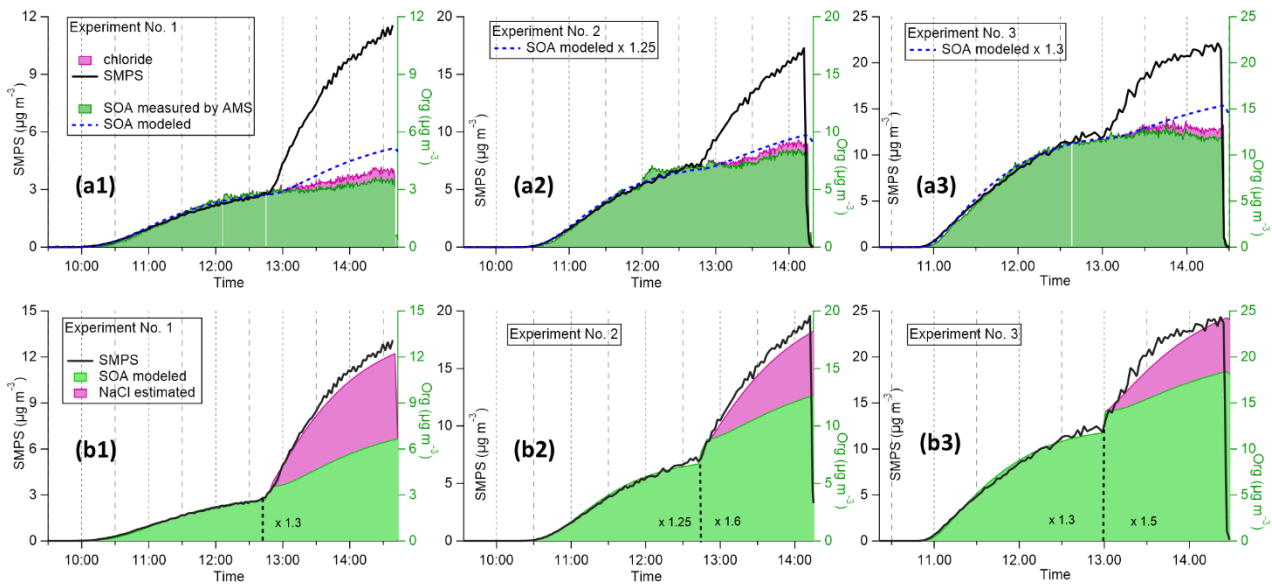
85 Parameters of the corresponding physical process were given at the bottom part of Table S1. The injection rate of α -pinene and O₃ are determined by their concentration in the total inflow as the only source. The flush-out rate is determined according to their instant concentration and the total flush-out flow rate (as in Fig. 2b), which is similar for α -pinene, O₃, and NO_x but is relatively a slow process for HOM related molecules (e.g. RO₂, RO, or closed-shell products) comparing to other sinks. Five tests with either O₃ or NO₂ were conducted to fit their decay (i.e. flush-out) rate constant k_{flushout} ($= 0.0033 \pm 0.0001$ s⁻¹), which is quite consistent with the residential time within the COALA chamber ($50 \text{ min}^{-1} = 0.0033 \text{ s}^{-1}$, 2 m³ chamber with 40 LMP total flow). This result indicates that the COALA chamber was well mixed. The loss rate of HOM onto pre-existed particles (i.e. condensation sink, k_{CS_HOM}) was estimated using SMPS measured size distribution of total aerosol particles for each experiment (Dal Maso et al., 2002). The diffusion coefficient of HOM vapors was estimated according to (Tang et al., 2015; Fuller et al., 1966), with ~ 0.045 and ~ 0.03 cm² s⁻¹ for monomers and dimers, respectively. However, this parameter only considers the kinetics of HOM vapors, while the volatility also plays an important role in the overall uptake. It has been reported that some HOM monomers are probably located in the SVOC range, and thus may re-evaporate after their condensation (Kurten et al., 2016). In fact, the decrease of D/M in the gas phase after adding seed particles in this work indicate that even when higher CS was calculated for monomers kinetically,

100 the dimers condensed more efficiently because of lower volatility (Fig. S7d). The loss rate onto the chamber walls ($k_{\text{wall_HOM}}$) was determined after the end of one experiment, during which the measurements continued for another half an hour after we stopped the injection of O_3 and AP. Thus, the wall loss rate, being $\sim 0.002 \text{ s}^{-1}$, was estimated by taking the difference between the total loss rate of HOM and previously determined loss rates ($k_{\text{wall_HOM}} = k_{\text{total}} - k_{\text{flushout}} - k_{\text{CS_HOM}}$).

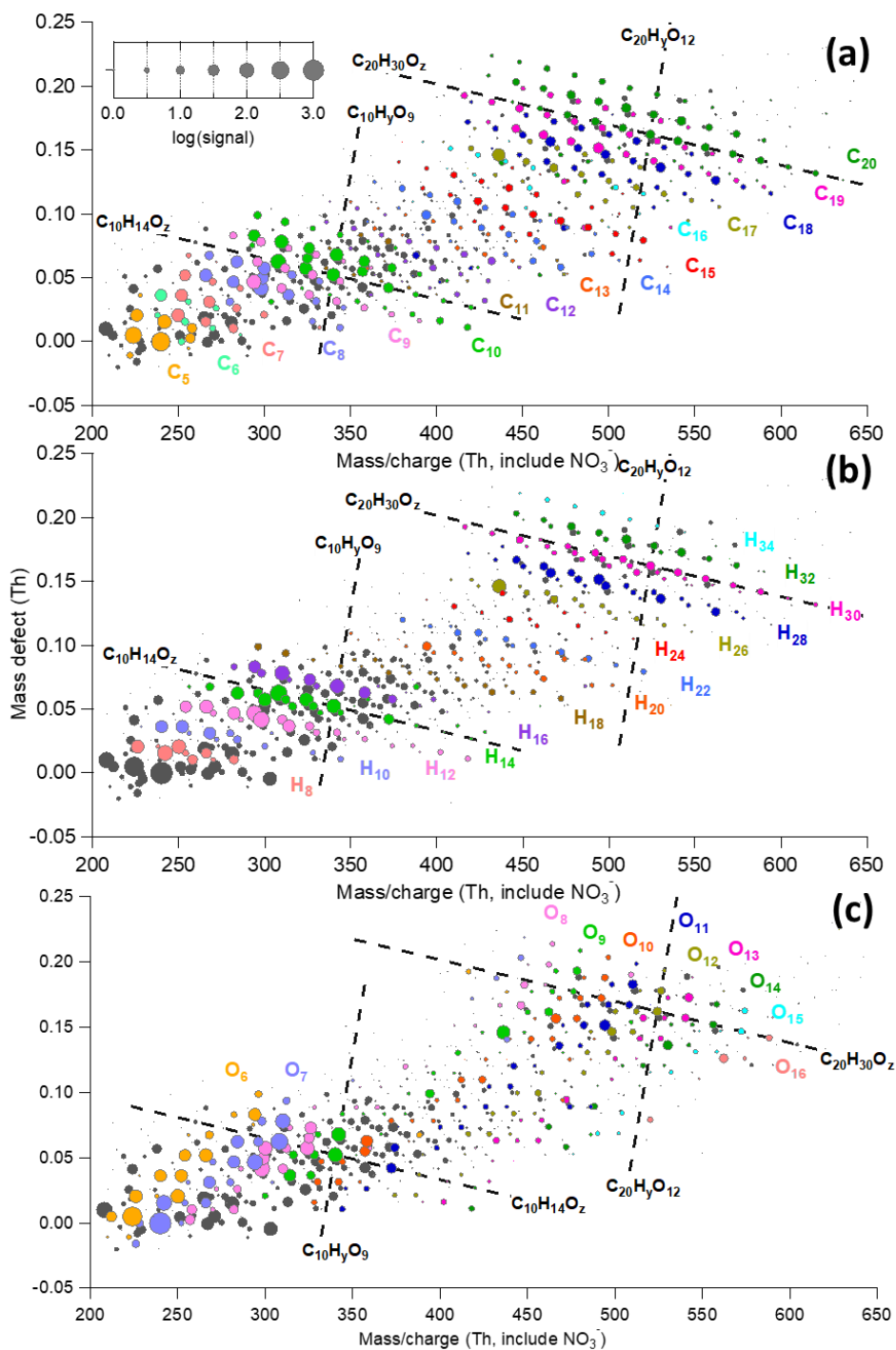
105 The SOA mass concentration was predicted to be solely due to the condensation of gas-phase HOM. Without measurements that constrain S/IVOC (thus not included in this simple box model), HOM species were expected to dominate SOA formation under low SOA conditions (which is the case for experiments conducted in this work, Sec. S2). Thus, we assigned the excess SOA mass to condensation of other vapors which are not HOM. The loss rate ($k_{\text{total}} = k_{\text{flushout}} + k_{\text{wall_SOA}}$) was determined during two decay tests, with values lower than the flush-out rate ($0.00025 \sim 0.00032 < 0.00033, \text{ s}^{-1}$), which indicates that the re-evaporation of S/IVOC from the chamber wall may contribute only slightly to the SOA mass. In addition, all potential chemical degradation/aging of HOM in both the gas and particle phases were not considered in this simple box model. Overall, we only included the flush-out as the sink for SOA particles (i.e. the direct wall loss and heterogeneous/particle phase loss of SOA were not investigated or regarded as negligible in this work).

115 **Table S1.** α -pinene (AP) reactions, rate constants, and physical parameters used in this work.

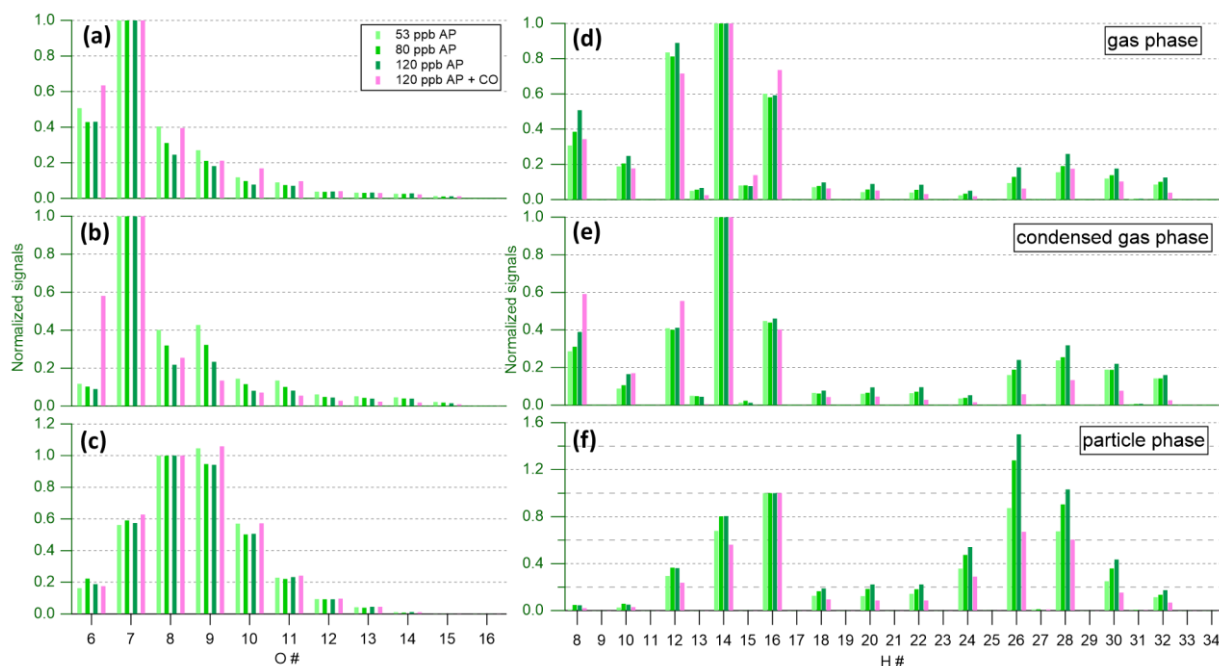
#	Reaction	Rate constant
	$\text{AP} + \text{O}_3 \rightarrow 0.2*\text{RO}_2 + 0.7*\text{RO}_4 + 0.01*\text{RO}_6 + 0.06*\text{RO}_8 + 0.03*\text{RO}_{10} + 0.8*\text{OH} + 0.001*\text{HO}_2$	$8.4\text{e-}17$
	$\text{AP} + \text{OH} \rightarrow 0.01\text{RO}_8 + 0.01*\text{RO}_{10} + 0.98*\text{RO}_2$	$5.3\text{e-}11$
	$\text{AP} + \text{NO}_3 \rightarrow \text{RO}_2\text{-NO}_3$	$6.2\text{e-}12$
	$\text{RO}_{6,8,10} \rightarrow \text{HOM_Monomers (H-shift)}$	0.05
	$\text{RO}_4 \rightarrow \text{other products}$	0.05
	$\text{RO}_2\text{-NO}_3 \rightarrow \text{pinonaldehyde} + \text{NO}_2$	0.1
	$\text{RO}_{6,8,10} + \text{RO}_{6,8,10} = a1*\text{HOM_Dimers} + (1-a1)*\text{HOM_Monomers}$	$8\text{e-}11$
	$\text{RO}_4 + \text{RO}_{6,8,10} = a2*\text{HOM_Dimers} + b2*\text{HOM_Monomers} + (1-a2-b2)*\text{RO}$	$2\text{e-}11$
	$\text{RO}_{6,8,10} + \text{HO}_2 = a3*\text{HOM_Monomers} + (1-a3)*\text{HOM_MonomersHO}_2$	$1\text{e-}11$
	$\text{RO}_{6,8,10} + \text{NO} = a4*\text{HOM_MonomersN} + (1-a4)*\text{other}$	$1\text{e-}11$
	k_{flushout}	$3.3\text{e-}3$
	$k_{\text{CS_HOM}}$	$5\text{e-}3 \sim 1.3\text{e-}2$
	$k_{\text{wall_HOM}}$	$5\text{e-}3$



120 **Figure S1.** Time series of particle phase measurements of experiment No. 1-3. **(a1-a3)** Integrated mass based on SMPS measurements (assuming a density of 1.5 g cm^{-3}), organic and chloride mass concentrations from AMS measurements. The blue dashed line shows the modeled SOA formed by the condensation of HOM vapors. **(b1-b3)** Reconstructed NaCl and SOA mass concentrations from the method described in Section S1.



125 **Figure S2.** Mass defect plot of gas phase signals (30-min average) measured in experiment No. 3 (input flow concentration as 120 ppb α -pinene and 33 ppb O₃). The data points are identical in each panel, except for the coloring. The points are colored by (a) carbon number, (b) hydrogen number, and (c) oxygen number. The marker size is proportional to the logarithm scale of measured raw signals. The uncolored markers (grey) are either unknown peaks (unidentified) or not HOM compounds according to the nomenclature of “HOM” (Bianchi et al., 2019).



130

Figure S3. The distribution of HOM products, grouped by (left) oxygen numbers and (right) hydrogen numbers for the (a, d) gas phase, (b, e) condensed (without seed – with seed) gas phase, and (c, f) particle phase, respectively. Note that the gas phase O family distributions are normalized by O₇ while O₈ is used for the particle phase measurements. The gas phase H family distributions are normalized by H₁₄ while H₁₆ is used for the particle phase measurements.

135

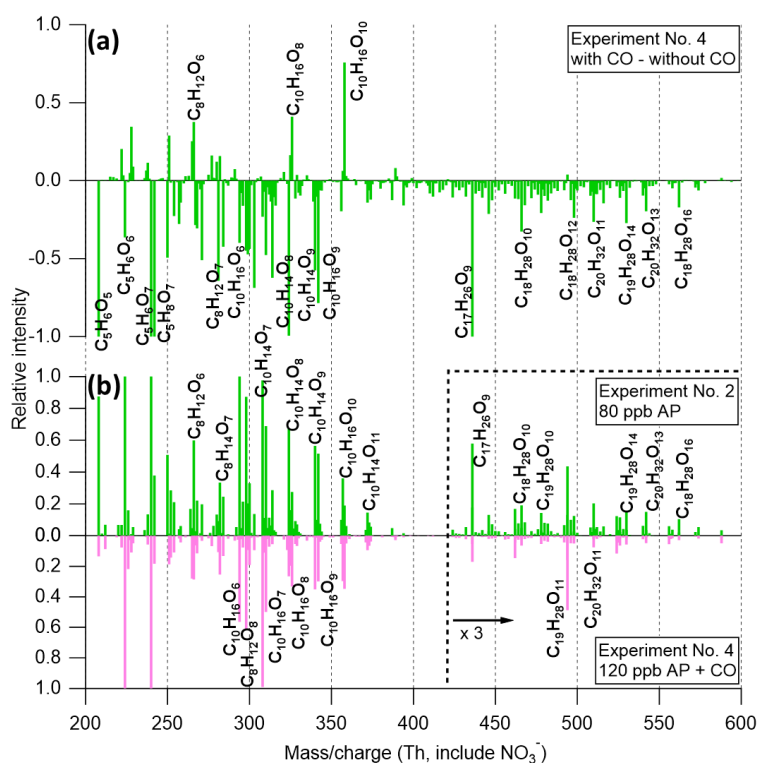


Figure S4. (a) The difference of gas phase mass spectra (30-min average) observed with and without CO in experiment No.4, normalized to (C₁₀H₁₄O₈)NO₃ at m/z 324 with m/z 208, 240, and 242 off the scale. (b) Comparison of gas phase mass spectra observed without CO (green) in experiment No.1 (53 ppb α -pinene) and with CO (pink) in experiment No.4 (120 ppb α -pinene with CO), normalized to (C₁₀H₁₄O₇)NO₃ at m/z 308 with m/z 224 and 240 off the scale. The signals with m/z larger than 420 was scaled by a factor of 3.

140

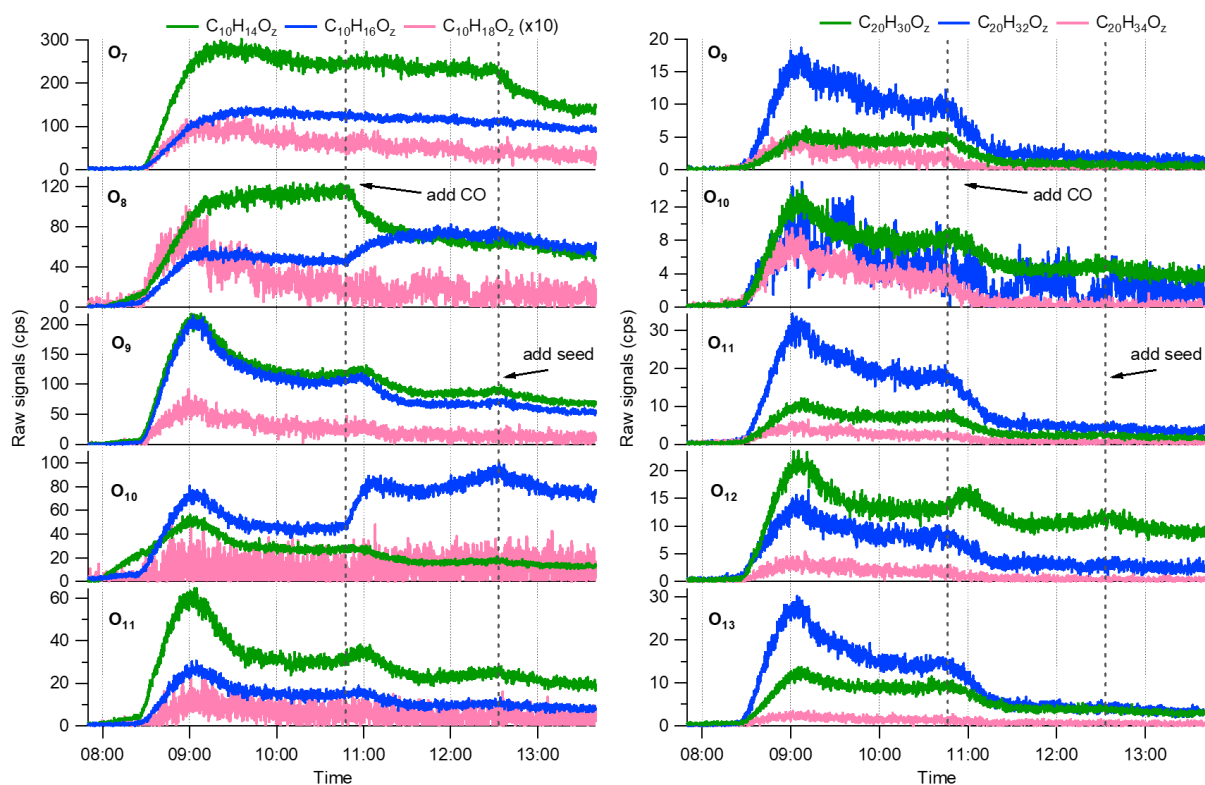


Figure S5. Time series (10s-averaged data points) of (left) $C_{10}H_{14,16,18}O_z$ and (right) $C_{20}H_{30,32,34}O_z$ measured in the gas phase from experiment No. 4 (120 ppb α -pinene, 33 ppb O_3 with 100 ppm CO).

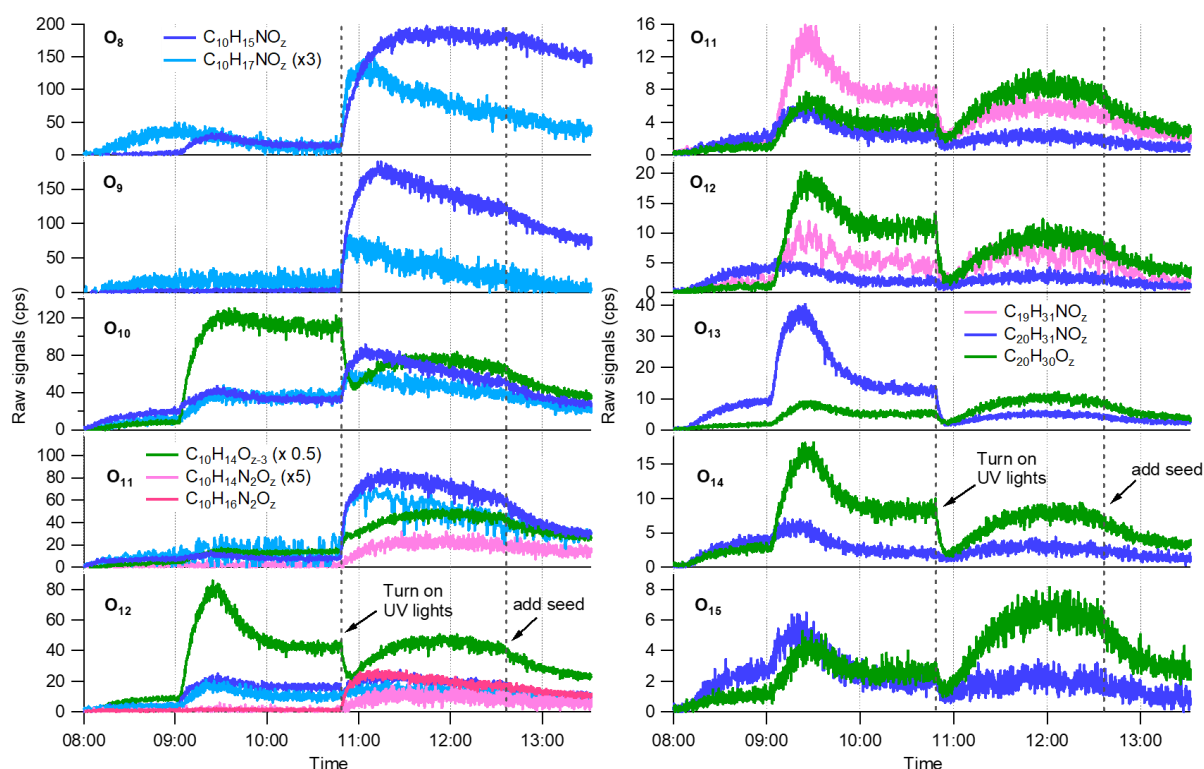
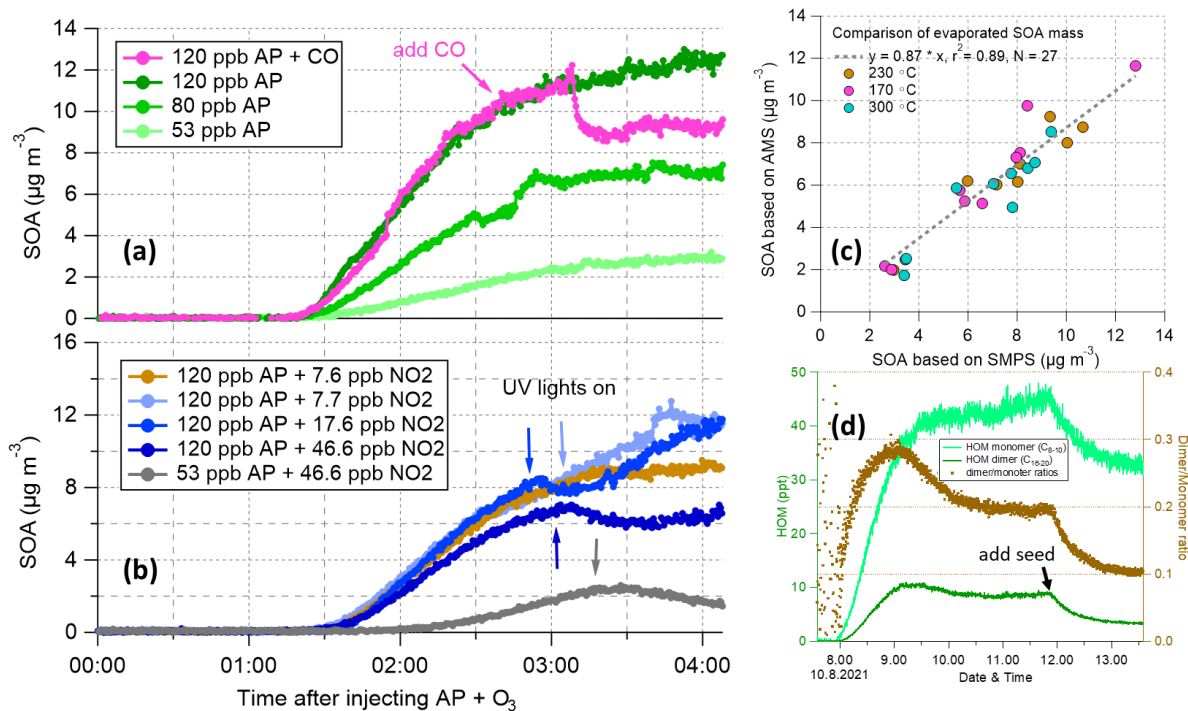


Figure S6. Time series (10s averaged data points) of main/selected (left) monomers and (right) dimers measured in the gas phase of experiment No. 7 (120 ppb α -pinene, 33 ppb O_3 , and 17.3 ppb NO_2).



150

Figure S7. (a, b) time series (20s averaged data points) of SOA measured by AMS for each experiment. (c) Comparison of evaporated SOA mass (i.e. the difference between VIA and bypass modes) between AMS and SMPS measurements. (d) Time series of gas-phase HOM monomers and dimers as well as the dimer/monomer ratio measured in experiment No. 1 (input flow with 53 ppb α -pinene and 33 ppb O_3).

155

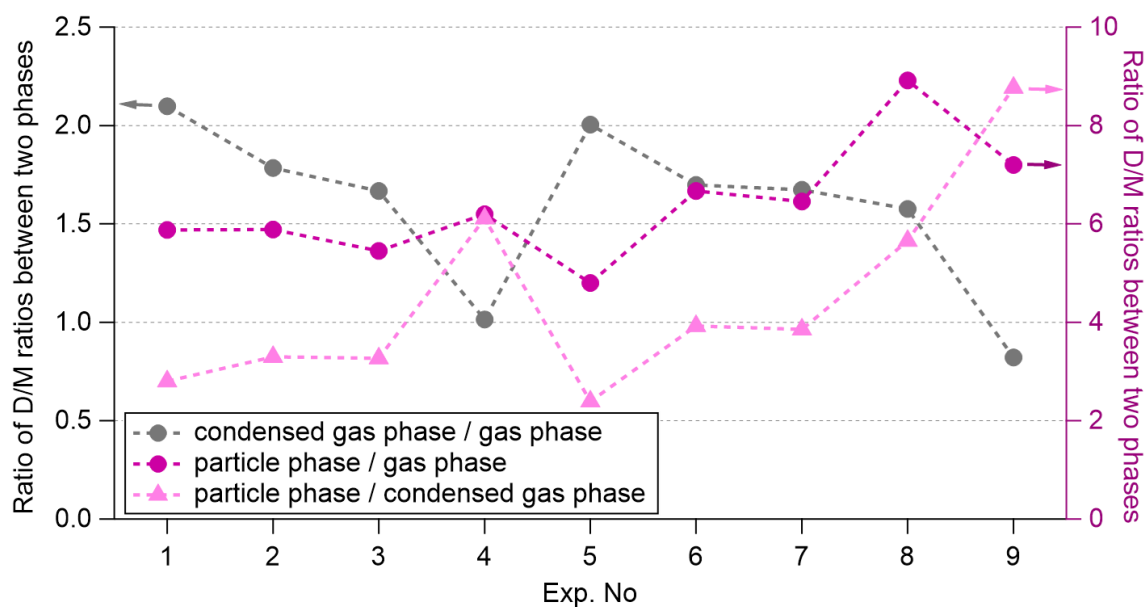


Figure S8. Ratio of D/M ratios obtained between different phases (using the same dataset as used in Figure. 8c).

160

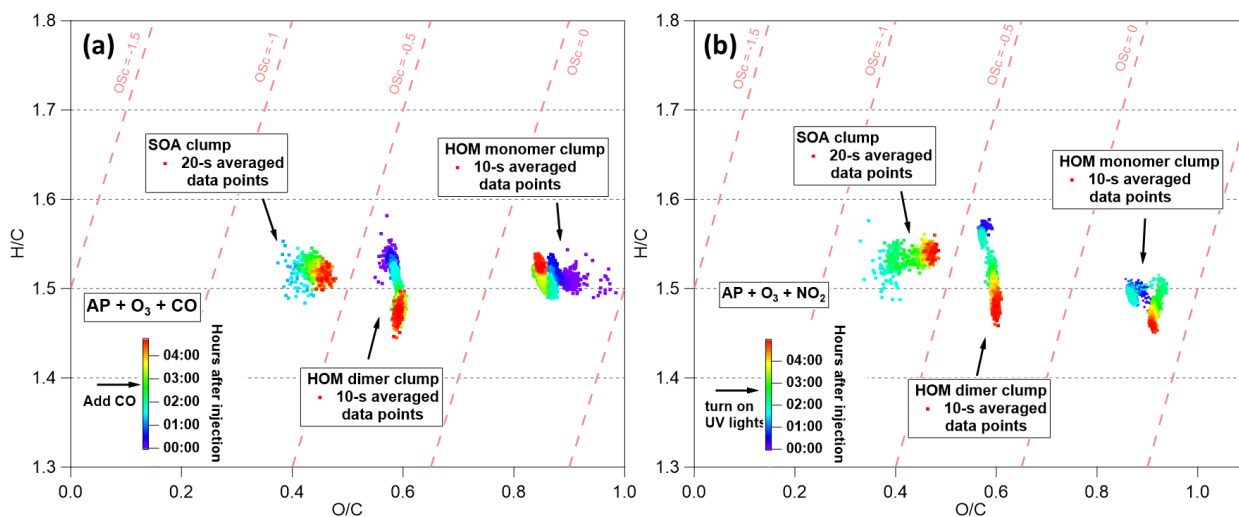
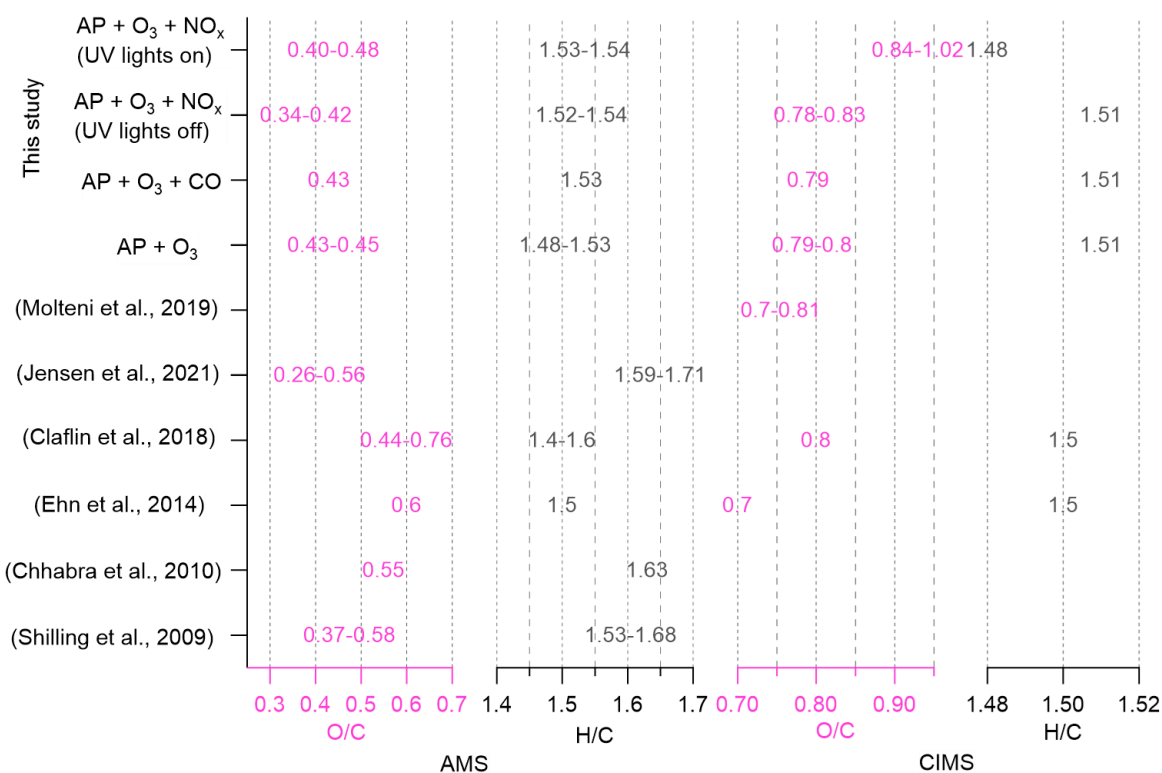


Figure S9. Van Krevelen diagram of datasets from experiment (a) No. 4 and (b) No. 7. The gas-phase HOM (separated into monomers and dimers) and SOA measurements are colored by the time after α -pinene and O₃ injection.



165

Figure S10. Summary of elemental ratios of SOA and HOM (formed from ozonolysis of α -pinene under various conditions) measured in both the gas and particle phases. The detailed description is given in Table S4.

170

Table S2. Comparison of main particle-phase compounds (by α -pinene and O_3 reactions) identified by a NO_3 -CIMS used in this work and other techniques. The chemical formula of main monomers and dimers are roughly listed according to their relative abundance in SOA (e.g. O numbers), if the concentration was measured/reported.

This work	(Müller et al., 2009)	(Kristensen et al., 2020)	(Zhang et al., 2015)	(Pospisilova et al., 2020)
NO_3 -CIMS	^a HPLC/FTICR-MS	^b UHPLC/ESI-qToF-MS	UHPLC/ESI-qToF-MS	^c EESI-TOF
Monomer				
$C_{10}H_{16}O_{9,8,7,10,6}$	$C_{10}H_{16}O_{4,5,6}$	$C_{10}H_{16}O_{3,4,6}$	$C_{10}H_{16}O_{3,4,6}$	$C_{10}H_{16}O_{6,5,4,7,3,8}$
$C_{10}H_{14}O_{8,9,10,7}$	/	$C_{10}H_{14}O_{4,5}$	$C_{10}H_{14}O_{4,5}$	$C_{10}H_{14}O_8$
$C_9H_{14}O_{7,8,9}$	$C_9H_{14}O_{5,6}$	$C_9H_{14}O_{4,3,5}$	$C_9H_{14}O_{3,4}$	$C_9H_{14}O_{4,5}$
$C_8H_{12}O_{7,6}$	$C_8H_{12}O_{4,5,6}$	$C_8H_{12}O_{4,6}$	$C_8H_{12}O_4$	$C_8H_{12}O_4$
$C_9H_{12}O_{6,8}$	$C_9H_{12}O_4$	/	/	/
$C_8H_{14}O_6$	$C_8H_{14}O_{4,5}$	$C_8H_{14}O_{5,6}$	$C_8H_{14}O_5$	/
Dimer				
$C_{17}H_{26}O_{8,9,7,10}$	$C_{17}H_{26}O_{6,7,8}$	$C_{17}H_{26}O_{8,7,5,9}$	$C_{17}H_{26}O_{5,6,8}$	$C_{17}H_{26}O_{8,7}$
$C_{19}H_{28}O_{9,10,8,11}$	$C_{19}H_{28}O_7$	$C_{19}H_{28}O_{7,6,5,8,9}$	$C_{19}H_{28}O_{7,9}$	$C_{19}H_{28}O_9$
$C_{18}H_{28}O_{9,8,10,11}$	$C_{18}H_{28}O_{6,7,8}$	$C_{18}H_{28}O_{6,7,8,9}$	$C_{18}H_{28}O_7$	/
$C_{16}H_{26}O_{7,8,9}$	$C_{16}H_{26}O_{6,7}$	$C_{16}H_{26}O_{6,7,9,10}$	$C_{16}H_{26}O_6$	$C_{16}H_{26}O_7$
$C_{16}H_{24}O_{8,9,7}$	$C_{16}H_{24}O_8$	$C_{16}H_{24}O_{6,7,8}$	$C_{16}H_{24}O_{6,8}$	/
$C_{18}H_{26}O_{9,10,8}$	/	/	$C_{18}H_{26}O_8$	/
$C_{19}H_{30}O_{9,10}$	$C_{19}H_{30}O_7$	$C_{19}H_{30}O_{8,5,6,7}$	/	$C_{19}H_{30}O_8$
$C_{17}H_{24}O_9$	/	/	/	/
$C_{17}H_{28}O_{9,8}$	/	$C_{17}H_{28}O_{7,8}$	$C_{17}H_{28}O_9$	/
$C_{18}H_{30}O_{9,10}$	/	$C_{18}H_{30}O_{10}$	/	/
$C_{20}H_{30}O_{9,10,11,12}$	/	/	/	/
$C_{20}H_{32}O_{10,9,11,8}$	/	/	/	$C_{20}H_{32}O_{9,10,11}$

175 Notes:

^aHPLC/FTICR-MS: High-Performance Liquid Chromatography and Fourier Transform Ion Cyclotron Resonance-Mass Spectrometry.

^bUHPLC/ESI-qToF-MS: Ultra-High Performance Liquid Chromatography/Electrospray Ionization Quadrupole Time-of Flight Mass Spectrometry.

180 ^cEESI-TOF: Extractive Electrospray Ionization Time-Of-Flight Mass Spectrometer.

^dDerivatization with 2,4-dinitrophenylhydrazine (DNPH).

185

190

195 **Table S3.** Comparison of particle phase N-containing compounds (by α -pinene and NO_3 reactions) measured by a NO_3 -CIMS used in this work and other techniques. The chemical formula of main monomers and dimers are roughly listed according to their relative abundance in SOA (e.g. O numbers), if the concentration was measured/reported.

This work, NO_3 -CIMS		(Nah et al., 2016)	
α -pinene, monomer		^a FIGAERO-I-CIMS	
lights off	lights on	b-pinene + NO_3	α -pinene + NO_3
$\text{C}_9\text{H}_{15}\text{NO}_{9,10,8,7}$	$\text{C}_9\text{H}_{15}\text{NO}_{10,8,9,7}$	$\text{C}_9\text{H}_{15}\text{NO}_{7,8,9,6}$	/
$\text{C}_{10}\text{H}_{17}\text{NO}_{10,11,12,9,8}$	$\text{C}_{10}\text{H}_{17}\text{NO}_{9,10,8,11}$	$\text{C}_{10}\text{H}_{17}\text{NO}_{8,7,9,6,5,4}$	/
$\text{C}_{10}\text{H}_{15}\text{NO}_{11,8,10,9,12}$	$\text{C}_{10}\text{H}_{15}\text{NO}_{8,10,9,11,12,7}$	$\text{C}_{10}\text{H}_{15}\text{NO}_{6,8,7,5,9}$	$\text{C}_{10}\text{H}_{15}\text{NO}_{6,9,5}$
$\text{C}_9\text{H}_{13}\text{NO}_{9,8,7,10,11}$	$\text{C}_9\text{H}_{13}\text{NO}_{9,8,7,10}$	$\text{C}_9\text{H}_{13}\text{NO}_{7,8,9,6}$	$\text{C}_9\text{H}_{13}\text{NO}_6$
$\text{C}_{10}\text{H}_{19}\text{NO}_{8,9,10}$	/	$\text{C}_{10}\text{H}_{19}\text{NO}_{5,6,7,8}$	/
$\text{C}_8\text{H}_{11}\text{NO}_{9,10,7,8}$	$\text{C}_8\text{H}_{11}\text{NO}_{8,7,9,10}$	$\text{C}_8\text{H}_{11}\text{NO}_{7,6,8,9}$	/
$\text{C}_8\text{H}_{13}\text{NO}_{9,10,7,8}$	$\text{C}_8\text{H}_{13}\text{NO}_{9,10,7,8}$	$\text{C}_8\text{H}_{13}\text{NO}_{7,6,8}$	/
$\text{C}_{10}\text{H}_{18}\text{N}_2\text{O}_{11,12}$	/	/	/
$\text{C}_{10}\text{H}_{16}\text{N}_2\text{O}_{12,13,14}$	$\text{C}_{10}\text{H}_{16}\text{N}_2\text{O}_{12,13,14}$	/	$\text{C}_{10}\text{H}_{16}\text{N}_2\text{O}_7$
/	$\text{C}_{10}\text{H}_{14}\text{N}_2\text{O}_{12,11}$	/	/
/	$\text{C}_{10}\text{H}_{13}\text{NO}_{9,8,10}$	$\text{C}_{10}\text{H}_{13}\text{NO}_{6,7,8,9}$	/
α -pinene, dimer			
$\text{C}_{19}\text{H}_{31}\text{NO}_{11,12,13}$			
$\text{C}_{19}\text{H}_{29}\text{NO}_{10,12,8}$			
$\text{C}_{20}\text{H}_{31}\text{NO}_{12,11,13,10}$			
$\text{C}_{17}\text{H}_{25}\text{NO}_{10}$			
$\text{C}_{17}\text{H}_{27}\text{NO}_{10,11,12}$			
$\text{C}_{18}\text{H}_{29}\text{NO}_{10,11,12}$			
$\text{C}_{20}\text{H}_{33}\text{NO}_{12,11,13,10}$			
$\text{C}_{20}\text{H}_{29}\text{NO}_{12,13,10,11}$			
$\text{C}_{19}\text{H}_{27}\text{NO}_{12,11,10}$			

Notes:

200 ^aFIGAERO-I-CIMS: Filter Inlet for Gas and AEROSol – Iodide – Chemical Ionization Mass Spectrometer.

205

210

215 **Table S4.** Summary of elemental ratios of SOA and HOM (formed from ozonolysis of α -pinene under various conditions) measured in both the gas and particle phases.

description	gas phase CI-APi-TOF		particle phase AMS				references
	H/C	O/C	H/C	O/C	SOA	method	
AP + O ₃	/	/	1.38- 1.51	0.29- 0.46	0.5-140	AA	(Shilling et al., 2009)
	/	/	1.47	0.43	57-183	AA	(Chhabra et al., 2010)
	1.5	0.7	1.5	0.6	5-10	IA	(Ehn et al., 2014)
	1.5	0.8	1.4-1.6	0.44- 0.76	/	IA	(Claflin et al., 2018)
	/	/	1.59- 1.71	0.26- 0.56	6-100	IA	(Jensen et al., 2021)
	/	0.7-0.81	/	/	/	/	(Molteni et al., 2019)
	1.51	0.79-0.8	1.48- 1.53	0.43- 0.45	3-15	IA	This study
AP + O ₃ + CO	1.51	0.79	1.53	0.43	~10	IA	This study
AP + O ₃ + NO _x	1.51	0.78- 0.83	1.52- 1.54	0.34- 0.42	3-10	IA	This study (lights off)
AP + O ₃ + NO _x	1.48	0.84- 1.02	1.53- 1.54	0.40- 0.48	2-15	IA	This study (lights on)

Notes: elemental ratios adopted from previous studies using the AA method (Aiken et al., 2008) could be converted to IA methods by scaling an empirical factor of 1.27 and 1.11 for O/C and H/C ratios, respectively (Canagaratna et al., 2015), in Figure S10. SOA mass in above table was given in unit of $\mu\text{g m}^{-3}$.

220

225

230

235

Reference:

- Aiken, A. C., Decarlo, P. F., Kroll, J. H., Worsnop, D. R., Huffman, J. A., Docherty, K. S., Ulbrich, I. M., Mohr, C., Kimmel, J. R., and Sueper, D.: O/C and OM/OC ratios of primary, secondary, and ambient organic aerosols with high-resolution time-of-flight aerosol mass spectrometry, *Environ. Sci. Technol.*, 42, 4478-4485, <https://doi.org/10.1021/es703009q>, 2008.
- 240 Berndt, T., Mentler, B., Scholz, W., Fischer, L., Herrmann, H., Kulmala, M., and Hansel, A.: Accretion Product Formation from Ozonolysis and OH Radical Reaction of α -Pinene: Mechanistic Insight and the Influence of Isoprene and Ethylene, *Environ. Sci. Technol.*, 52, 11069-11077, doi:10.1021/acs.est.8b02210, 2018.
- 245 Bianchi, F., Kurtén, T., Riva, M., Mohr, C., Rissanen, M. P., Roldin, P., Berndt, T., Crouse, J. D., Wennberg, P. O., Mentel, T. F., Wildt, J., Junninen, H., Jokinen, T., Kulmala, M., Worsnop, D. R., Thornton, J. A., Donahue, N., Kjaergaard, H. G., and Ehn, M.: Highly Oxygenated Organic Molecules (HOM) from Gas-Phase Autoxidation Involving Peroxy Radicals: A Key Contributor to Atmospheric Aerosol, *Chem. Rev.*, 119, 3472-3509, doi:10.1021/acs.chemrev.8b00395, 2019.
- 250 Canagaratna, M. R., Jimenez, J. L., Kroll, J. H., Chen, Q., Kessler, S. H., Massoli, P., Hildebrandt Ruiz, L., Fortner, E., Williams, L. R., Wilson, K. R., Surratt, J. D., Donahue, N. M., Jayne, J. T., and Worsnop, D. R.: Elemental ratio measurements of organic compounds using aerosol mass spectrometry: characterization, improved calibration, and implications, *Atmos. Chem. Phys.*, 15, 253-272, doi:10.5194/acp-15-253-2015, 2015.
- 255 Chhabra, P. S., Flagan, R. C., and Seinfeld, J. H.: Elemental analysis of chamber organic aerosol using an aerodyne high-resolution aerosol mass spectrometer, *Atmos. Chem. Phys.*, 10, 4111-4131, doi:10.5194/acp-10-4111-2010, 2010.
- Clafin, M. S., Krechmer, J. E., Hu, W., Jimenez, J. L., and Ziemann, P. J.: Functional Group Composition of Secondary Organic Aerosol Formed from Ozonolysis of α -Pinene Under High VOC and Autoxidation Conditions, *ACS Earth and Space Chemistry*, 2, 1196-1210, doi:10.1021/acsearthspacechem.8b00117, 2018.
- 260 Dal Maso, M., Kulmala, M., Lehtinen, K. E. J., Mäkelä, J. M., Aalto, P., and O'Dowd, C. D.: Condensation and coagulation sinks and formation of nucleation mode particles in coastal and boreal forest boundary layers, *J. Geophys. Res.- Atmos.*, 107, PAR 2-1-PAR 2-10, <https://doi.org/10.1029/2001JD001053>, 2002.
- 265 Ehn, M., Thornton, J. A., Kleist, E., Sipila, M., Junninen, H., Pullinen, I., Springer, M., Rubach, F., Tillmann, R., Lee, B., Lopez-Hilfiker, F., Andres, S., Acir, I. H., Rissanen, M., Jokinen, T., Schobesberger, S., Kangasluoma, J., Kontkanen, J., Nieminen, T., Kurten, T., Nielsen, L. B., Jorgensen, S., Kjaergaard, H. G., Canagaratna, M., Maso, M. D., Berndt, T., Petaja, T., Wahner, A., Kerminen, V. M., Kulmala, M., Worsnop, D. R., Wildt, J., and Mentel, T. F.: A large source of low-volatility secondary organic aerosol, *Nature*, 506, 476-479, doi:10.1038/nature13032, 2014.
- 270 Fuller, E. N., Schettler, P. D., and Giddings, J. C.: NEW METHOD FOR PREDICTION OF BINARY GAS-PHASE DIFFUSION COEFFICIENTS, *Industrial & Engineering Chemistry*, 58, 18-27, doi:10.1021/ie50677a007, 1966.
- Iyer, S., Rissanen, M. P., Valiev, R., Barua, S., Krechmer, J. E., Thornton, J., Ehn, M., and Kurtén, T.: Molecular mechanism for rapid autoxidation in α -pinene ozonolysis, *Nature communications*, 12, 878, doi:10.1038/s41467-021-21172-w, 2021.
- 275 Jensen, L. N., Canagaratna, M. R., Kristensen, K., Quéléver, L. L. J., Rosati, B., Teiwes, R., Glasius, M., Pedersen, H. B., Ehn, M., and Bilde, M.: Temperature and volatile organic compound concentrations as controlling factors for chemical composition of α -pinene-derived secondary organic aerosol, *Atmos. Chem. Phys.*, 21, 11545-11562, doi:10.5194/acp-21-11545-2021, 2021.
- 280 Jokinen, T., Berndt, T., Makkonen, R., Kerminen, V. M., Junninen, H., Paasonen, P., Stratmann, F., Herrmann, H., Guenther, A. B., Worsnop, D. R., Kulmala, M., Ehn, M., and Sipila, M.: Production of extremely low volatile organic compounds from biogenic emissions: Measured yields and atmospheric implications, *Proc. Natl. Acad. Sci. USA*, 112, 7123-7128, doi:10.1073/pnas.1423977112, 2015.
- 285 Kirkby, J., Duplissy, J., Sengupta, K., Frege, C., Gordon, H., Williamson, C., Heinritzi, M., Simon, M., Yan, C., Almeida, J., Trostl, J., Nieminen, T., Ortega, I. K., Wagner, R., Adamov, A., Amorim, A., Bernhammer, A. K., Bianchi, F., Breitenlechner, M., Brilke, S., Chen, X., Craven, J., Dias, A., Ehrhart, S., Flagan, R. C., Franchin, A., Fuchs, C., Guida, R., Hakala, J., Hoyle, C. R., Jokinen, T., Junninen, H., Kangasluoma, J., Kim, J., Krapf, M., Kurten, A., Laaksonen, A., Lehtipalo, K., Makhmutov, V., Mathot, S., Molteni, U., Onnela, A., Perakyla, O., Piel, F., Petaja, T., Praplan, A. P., Pringle, K., Rap, A., Richards, N. A., Riipinen, I., Rissanen, M. P., Rondo, L., Sarnela, N., Schobesberger, S., Scott, C. E., Seinfeld, J. H., Sipila, M., Steiner, G., Stozhkov, Y., Stratmann, F., Tome, A., Virtanen, A., Vogel, A. L., Wagner, A. C., Wagner, P. E., Weingartner, E.,
- 290 Wimmer, D., Winkler, P. M., Ye, P., Zhang, X., Hansel, A., Dommen, J., Donahue, N. M., Worsnop, D. R.,

- Baltensperger, U., Kulmala, M., Carslaw, K. S., and Curtius, J.: Ion-induced nucleation of pure biogenic particles, *Nature*, 533, 521-526, doi:10.1038/nature17953, 2016.
- 295 Kristensen, K., Jensen, L. N., Quéléver, L. L. J., Christiansen, S., Rosati, B., Elm, J., Teiwes, R., Pedersen, H. B., Glasius, M., Ehn, M., and Bilde, M.: The Aarhus Chamber Campaign on Highly Oxygenated Organic Molecules and Aerosols (ACCHA): particle formation, organic acids, and dimer esters from α -pinene ozonolysis at different temperatures, *Atmos. Chem. Phys.*, 20, 12549-12567, doi:10.5194/acp-20-12549-2020, 2020.
- 300 Kurten, T., Tiusanen, K., Roldin, P., Rissanen, M., Luy, J. N., Boy, M., Ehn, M., and Donahue, N.: alpha-Pinene Autoxidation Products May Not Have Extremely Low Saturation Vapor Pressures Despite High O:C Ratios, *The journal of physical chemistry. A*, 120, 2569-2582, doi:10.1021/acs.jpca.6b02196, 2016.
- Kurtén, T., Møller, K. H., Nguyen, T. B., Schwantes, R. H., Misztal, P. K., Su, L., Wennberg, P. O., Fry, J. L., and Kjaergaard, H. G.: Alkoxy Radical Bond Scissions Explain the Anomalously Low Secondary Organic Aerosol and Organonitrate Yields From α -Pinene + NO₃, *The Journal of Physical Chemistry Letters*, 8, 2826-2834, doi:10.1021/acs.jpcl.7b01038, 2017.
- 305 Mentel, T. F., Springer, M., Ehn, M., Kleist, E., Pullinen, I., Kurtén, T., Rissanen, M., Wahner, A., and Wildt, J.: Formation of highly oxidized multifunctional compounds: autoxidation of peroxy radicals formed in the ozonolysis of alkenes – deduced from structure–product relationships, *Atmos. Chem. Phys.*, 15, 6745-6765, doi:10.5194/acp-15-6745-2015, 2015.
- 310 Molteni, U., Simon, M., Heinritzi, M., Hoyle, C. R., Bernhammer, A.-K., Bianchi, F., Breitenlechner, M., Brilke, S., Dias, A., Duplissy, J., Frege, C., Gordon, H., Heyn, C., Jokinen, T., Kürten, A., Lehtipalo, K., Makhmutov, V., Petäjä, T., Pieber, S. M., Praplan, A. P., Schobesberger, S., Steiner, G., Stozhkov, Y., Tomé, A., Tröstl, J., Wagner, A. C., Wagner, R., Williamson, C., Yan, C., Baltensperger, U., Curtius, J., Donahue, N. M., Hansel, A., Kirkby, J., Kulmala, M., Worsnop, D. R., and Dommen, J.: Formation of Highly Oxygenated Organic Molecules from α -Pinene Ozonolysis: Chemical Characteristics, Mechanism, and Kinetic Model Development, *ACS Earth and Space Chemistry*, 3, 873-883, doi:10.1021/acsearthspacechem.9b00035, 2019.
- 315 Müller, L., Reinnig, M.-C., Hayen, H., and Hoffmann, T.: Characterization of oligomeric compounds in secondary organic aerosol using liquid chromatography coupled to electrospray ionization Fourier transform ion cyclotron resonance mass spectrometry, *Rapid Communications in Mass Spectrometry*, 23, 971-979, <https://doi.org/10.1002/rcm.3957>, 2009.
- 320 Nah, T., Sanchez, J., Boyd, C. M., and Ng, N. L.: Photochemical Aging of α -pinene and β -pinene Secondary Organic Aerosol formed from Nitrate Radical Oxidation, *Environ. Sci. Technol.*, 50, 222-231, doi:10.1021/acs.est.5b04594, 2016.
- Peräkylä, O., Riva, M., Heikkinen, L., Quéléver, L., Roldin, P., and Ehn, M.: Experimental investigation into the volatilities of highly oxygenated organic molecules (HOMs), *Atmos. Chem. Phys.*, 20, 649-669, doi:10.5194/acp-20-649-2020, 2020.
- 325 Pospisilova, V., Lopez-Hilfiker, F. D., Bell, D. M., El Haddad, I., Mohr, C., Huang, W., Heikkinen, L., Xiao, M., Dommen, J., Prevot, A. S. H., Baltensperger, U., and Slowik, J. G.: On the fate of oxygenated organic molecules in atmospheric aerosol particles, *Science Advances*, 6, eaax8922, doi:10.1126/sciadv.aax8922, 2020.
- 330 Bahreini R., Keywood M. D., Ng N. L., Varutbangkul V., Gao S., Flagan R. C., Seinfeld J. H., Worsnop D. R., and Jimenez J. L.: Measurements of Secondary Organic Aerosol from Oxidation of Cycloalkenes, Terpenes, and m-Xylene Using an Aerodyne Aerosol Mass Spectrometer, *Environ. Sci. Technol.*, 15, 5674–5688, <https://doi.org/10.1021/es048061a>, 2005.
- 335 Rissanen, M. P., Kurten, T., Sipila, M., Thornton, J. A., Kausiala, O., Garmash, O., Kjaergaard, H. G., Petaja, T., Worsnop, D. R., Ehn, M., and Kulmala, M.: Effects of chemical complexity on the autoxidation mechanisms of endocyclic alkene ozonolysis products: from methylcyclohexenes toward understanding alpha-pinene, *The journal of physical chemistry. A*, 119, 4633-4650, doi:10.1021/jp510966g, 2015.
- 340 Saunders, S. M., Jenkin, M. E., Derwent, R. G., and Pilling, M. J.: Protocol for the development of the Master Chemical Mechanism, MCM v3 (Part A): tropospheric degradation of non-aromatic volatile organic compounds, *Atmos. Chem. Phys.*, 3, 161-180, doi:10.5194/acp-3-161-2003, 2003.
- Schervish, M. and Donahue, N. M.: Peroxy radical chemistry and the volatility basis set, *Atmos. Chem. Phys.*, 20, 1183-1199, doi:10.5194/acp-20-1183-2020, 2020.
- 345 Shilling, J. E., Chen, Q., King, S. M., Rosenoern, T., Kroll, J. H., Worsnop, D. R., DeCarlo, P. F., Aiken, A. C., Sueper, D., and Jimenez, J. L.: Loading-dependent elemental composition of α -pinene SOA particles, *Atmos. Chem. Phys.*, 9, 771-782, <https://doi.org/10.5194/acp-9-771-2009>, 2009.
- Tang, M. J., Shiraiwa, M., Pöschl, U., Cox, R. A., and Kalberer, M.: Compilation and evaluation of gas phase diffusion coefficients of reactive trace gases in the atmosphere: Volume 2. Diffusivities of organic

- 350 compounds, pressure-normalised mean free paths, and average Knudsen numbers for gas uptake calculations, *Atmos. Chem. Phys.*, 15, 5585-5598, doi:10.5194/acp-15-5585-2015, 2015.
- Zhang, X., McVay, R. C., Huang, D. D., Dalleska, N. F., Aumont, B., Flagan, R. C., and Seinfeld, J. H.: Formation and evolution of molecular products in α -pinene secondary organic aerosol, *Proc. Natl. Acad. Sci. USA*, 112, 14168-14173, doi:10.1073/pnas.1517742112, 2015.
- 355 Zhao, Y., Thornton, J. A., and Pye, H. O. T.: Quantitative constraints on autoxidation and dimer formation from direct probing of monoterpene-derived peroxy radical chemistry, *Proc. Natl. Acad. Sci. USA*, 115, 12142-12147, doi:10.1073/pnas.1812147115, 2018.